CHAPTER IV
RESULTS AND DISCUSSION

4.1 Photocatalyst Characterizations

4.1.1 TG-DTA Results

The TG-DTA curves were used to study the thermal decomposition behavior of the synthesized dried perovskite photocatalysts and to obtain their suitable calcination temperature. Figure 4.1 shows the TG-DTA curves of the dried $MgTiO_3$, $CaTiO_3$, and $SrTiO_3$ gels synthesized by the sol-gel method, which was shown to provide the good quality photocatalyst (Puangpetch, *et al.*, 2008). The DTA curves show exothermic peaks, which can be divided into four regions. The details of the region of exothermic peaks and their corresponding weight losses are summarized in Table 4.1. The first region is attributed to the removal of physisorbed water and ethanol molecules. The second region is attributed to the burnout of the surfactant template. The third region is attributed to the removal of remnant carbons and chemisorbed water. The fourth region is attributed to the crystallization process of the photocatalyst and the decomposition of solvent that is tightly bonded in the molecular level with alkaline earth element (Mg, Ca, and Sr) and Ti metals in the gel network (Puangpetch, *et al.*, 2008). However, the temperature ranges of these regions of each perovskite photocatalyst are different because the interaction of each species in gel network may be different. The TG results reveal that the calcination temperature of approximately 500°C for the $MgTiO_3$ photocatalyst and 650°C for the $CaTiO_3$ and $SrTiO_3$ photocatalysts are sufficient for both surfactant template removal and complete photocatalyst crystallization. However, the calcination temperature in the range of 450 and 700°C is used to investigate its effect on crystallinity, surface area, and consequent photocatalytic hydrogen production activity.

Table 4.1 Thermal decomposition behavior of the dried synthesized perovskite $MgTiO_3$, $CaTiO_3$, and $SrTiO_3$ photocatalysts from TG-DTA analysis

Photocatalyst	Position of exothermic peak (°C)				Corresponding weight loss (wt.%)				
	1st region	2nd region	3rd region	4th region	1st region	2nd region	3rd region	4th region	Total
$MgTiO_3$	25-150	150-230	230-340	340-500	20.9	22.9	14.0	9.7	67.5
$CaTiO_3$	25-150	150-300	300-400	400-650	1.8	17.7	6.8	27.3	53.6
$SrTiO_3$	25-150	150-300	300-425	425-650	1.5	10.7	6.8	26.8	45.8

(a)

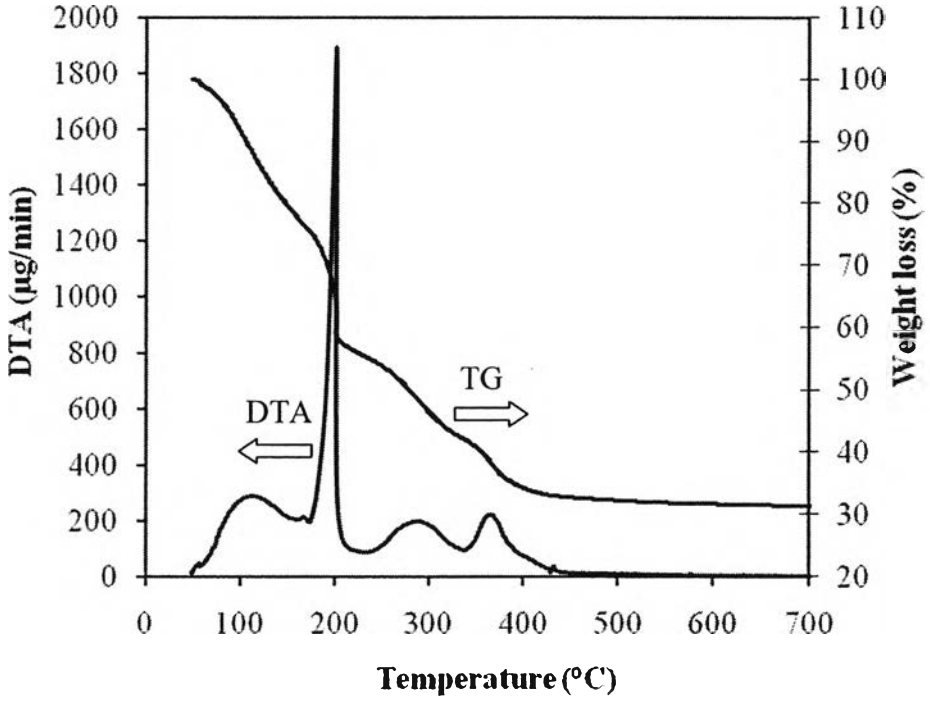

Figure 4.1 TG-DTA curves of the dried synthesized (a) $MgTiO_3$, (b) $CaTiO_3$, and (c) $SrTiO_3$ photocatalysts.

(b)

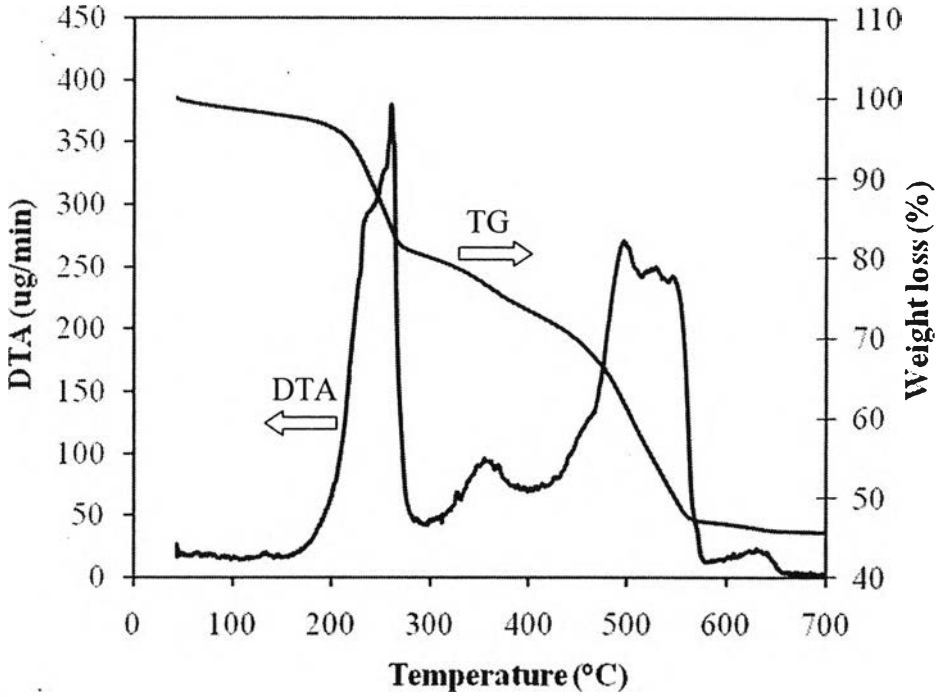

(c)

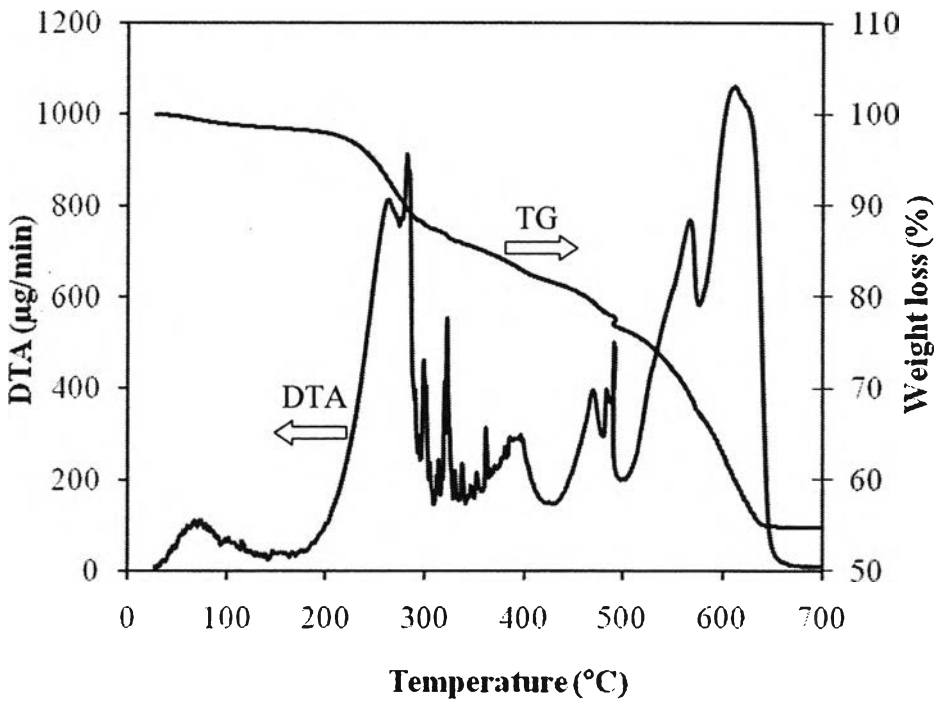

Figure 4.1 (Continued) TG-DTA curves of the dried synthesized (a) $MgTiO_3$, (b) $CaTiO_3$, and (c) $SrTiO_3$ photocatalysts.

4.1.2 N_2 Adsorption-Desorption Results

The N_2 adsorption-desorption analysis was used to verify the mesoporosity of the studied photocatalysts. The shape of the isotherms exhibits the characteristic behavior of the structure of powder, which is composed of an assembly of particles with large open packing. The adsorption-desorption isotherms of the synthesized $MgTiO_3$ photocatalyst calcined at 500°C, the $CaTiO_3$ photocatalyst calcined at 550°C, the $SrTiO_3$ photocatalyst calcined at 650°C, and the synthesized 0.5 wt.% Pt-loaded mesoporous-assembled $SrTiO_3$ photocatalyst calcined at 650°C are exemplified in Figure 4.2, whereas the adsorption-desorption isotherms of the commercial $SrTiO_3$ and P-25 TiO_2 photocatalysts are shown in Figure 4.3. The isotherms of all the synthesized photocatalysts exhibit typical IUPAC type IV-like pattern with a hysteresis loop, which is the characteristic of mesoporous material (mesoporous size between 2 and 50 nm) according to the classification of IUPAC (Rouquerol *et al.*, 1999). A sharp increase in adsorption volume of N_2 could be observed at high relative pressure. This sharp increase can be attributed to the capillary condensation of N_2 inside the mesopores, indicating the good homogeneity of the sample and fairly small pore size since the P/P_0 position of the inflection point is directly related to the pore dimension. The isotherms of the synthesized 0.5 wt.% Pt-loaded mesoporous-assembled $SrTiO_3$ photocatalyst also exhibit IUPAC type IV-like pattern with a hysteresis loop. This suggests that the Pt loading by the SSSG method did not significantly affect the mesoporous structure of the photocatalyst. Therefore, its mesoporous structure could be maintained. The isotherms of the commercial $SrTiO_3$ and P-25 TiO_2 photocatalysts, however, correspond to IUPAC type II pattern. They possess non-mesoporous characteristic due to the absence of a distinct hysteresis loop, indicating that their pore structure is mainly a macropore (pore diameter > 50 nm), and no capillary condensation of N_2 occurs inside the pores.

(a)

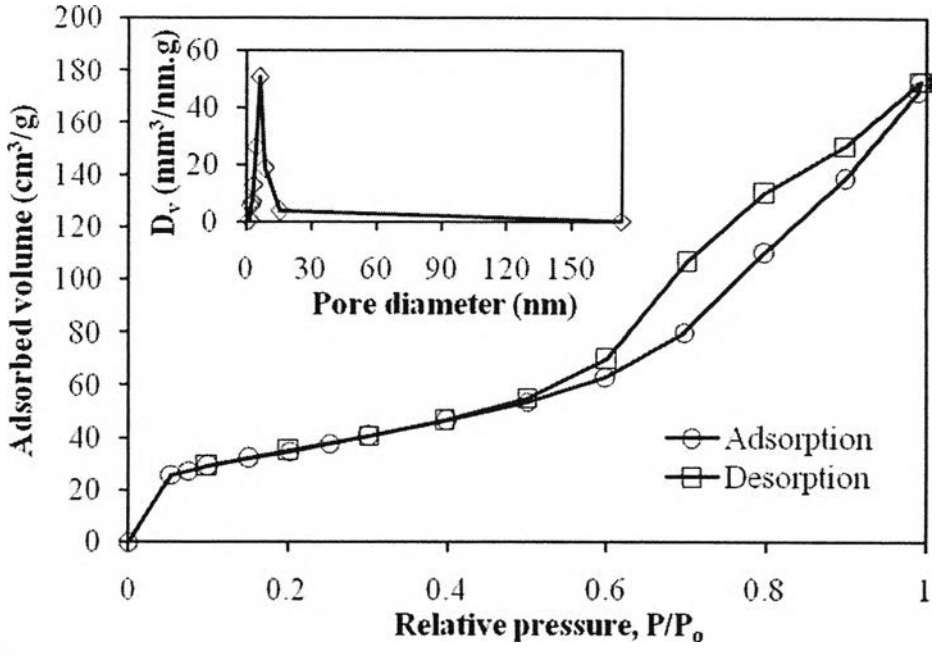

(b)

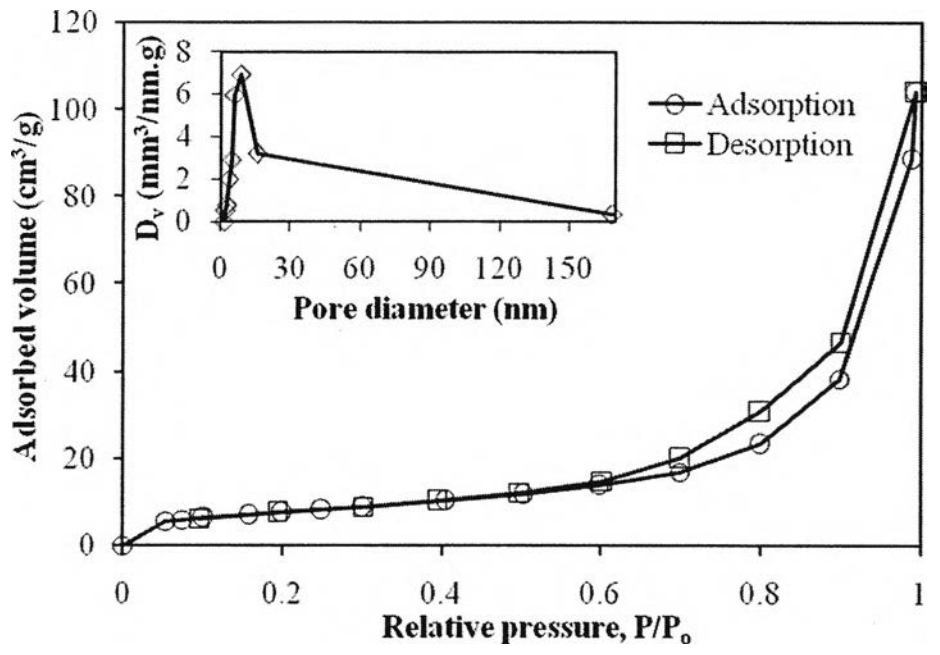

Figure 4.2 N_2 adsorption-desorption isotherms and pore size distributions (inset) of the synthesized (a) $MgTiO_3$ photocatalyst calcined at 500°C, (b) $CaTiO_3$ photocatalyst calcined at 550°C, (c) $SrTiO_3$ photocatalyst calcined at 650°C, and (d) the synthesized 0.5 wt.% Pt-loaded mesoporous-assembled $SrTiO_3$ photocatalyst calcined at 650°C.

(c)

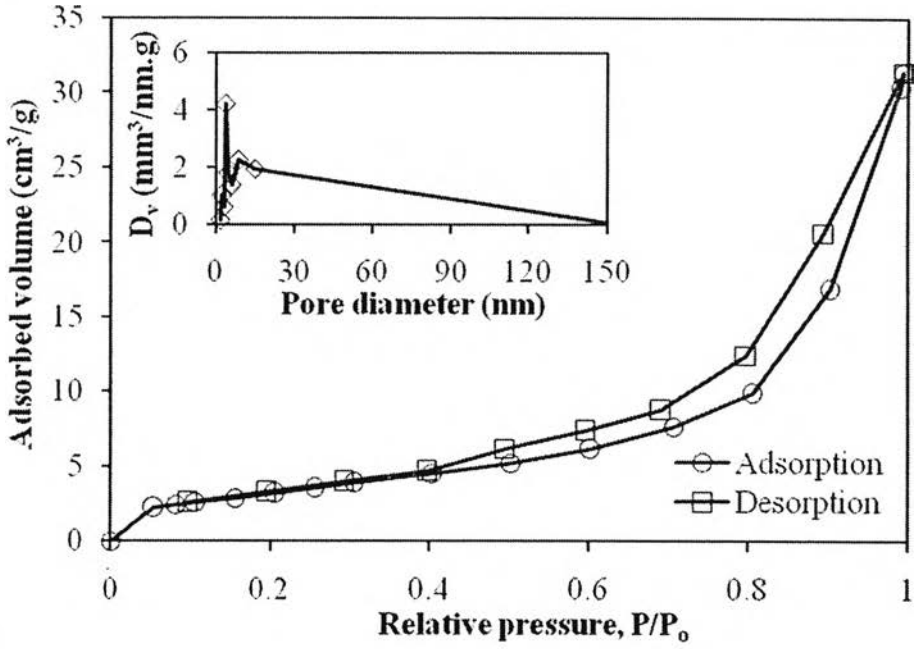

(d)

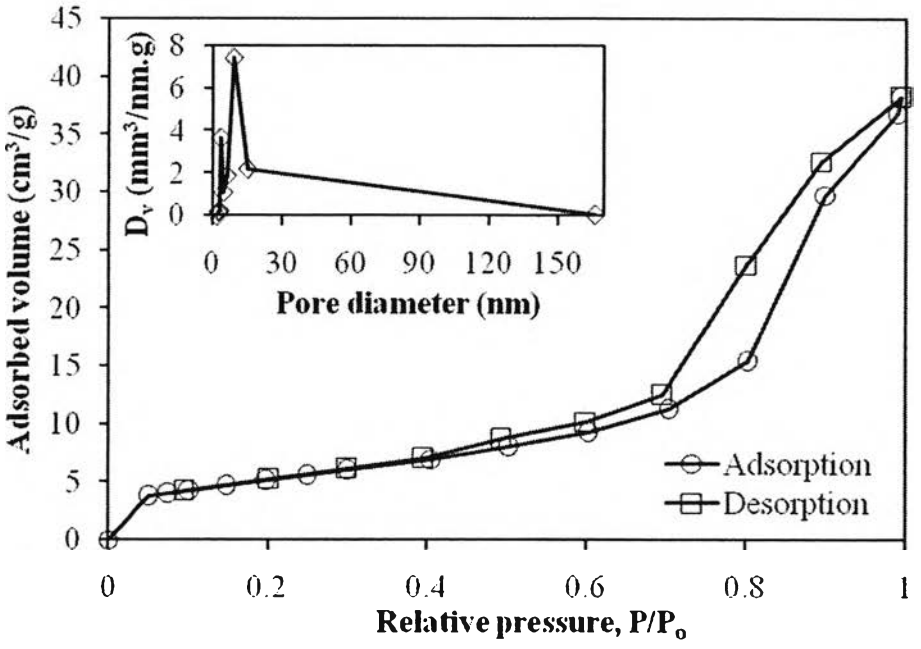

Figure 4.2 (Continued) N_2 adsorption-desorption isotherms and pore size distributions (inset) of the synthesized (a) $MgTiO_3$ photocatalyst calcined at 500°C, (b) $CaTiO_3$ photocatalyst calcined at 550°C, (c) $SrTiO_3$ photocatalyst calcined at 650°C, and (d) the synthesized 0.5 wt.% Pt-loaded mesoporous-assembled $SrTiO_3$ photocatalyst calcined at 650°C.

(a)

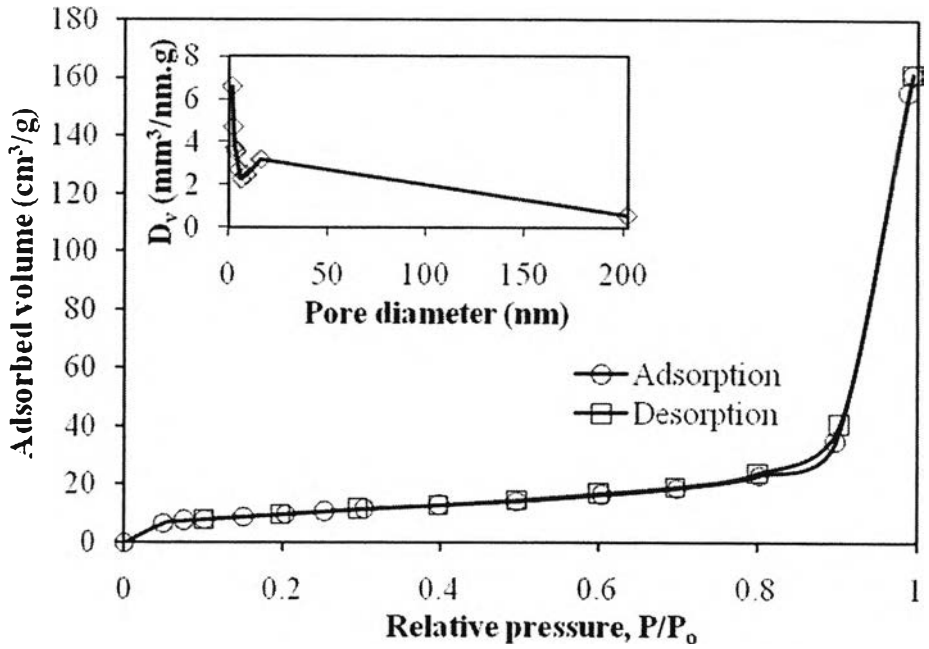

(b)

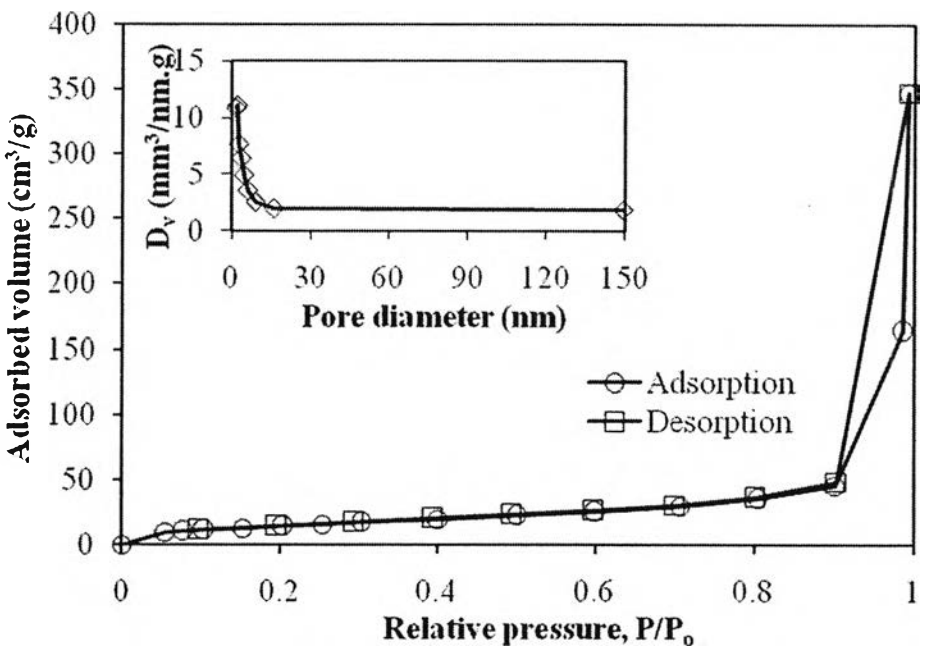

Figure 4.3 N_2 adsorption-desorption isotherms and pore size distributions (inset) of the commercial (a) $SrTiO_3$ and (b) P-25 TiO_2 photocatalysts.

The insets of Figure 4.2 and 4.3 show pore size distributions calculated from the desorption branch of the isotherms by the DH method. All the synthesized perovskite titanate photocatalysts, except the commercial $SrTiO_3$ and P-25 TiO_2 photocatalysts, possess narrow pore size distributions in the mesopore region (mesoporous size between 2 and 50 nm), whereas the pore size distributions of the commercial $SrTiO_3$ and P-25 TiO_2 photocatalysts are quite broad and are not mainly present in the mesoporous region. The textural properties obtained from N_2 adsorption-desorption isotherms, i.e. BET surface area, mean mesopore diameter, and total pore volume, of all the investigated photocatalysts are summarized in Table 4.2. As obviously seen, the surface area and total pore volume of all the synthesized photocatalysts tend to decrease with increasing calcination temperature, whereas the mean mesopore diameter of the synthesized $MgTiO_3$ and $CaTiO_3$ photocatalysts tends to increase; however, the mean mesopore diameter of the synthesized $SrTiO_3$ photocatalyst remains almost invariant. The synthesized photocatalysts have mean mesopore diameter located in the narrow range of 3 to 16 nm, identifying good quality of the samples. The perceived loss in surface area is explainable to pore coalescence due to crystallization of wall separating mesopores. Interestingly, the surface area of the 0.5 wt.% Pt-loaded mesoporous-assembled $SrTiO_3$ photocatalyst is higher than that of the unloaded $SrTiO_3$ at a calaination temperature of 650°C. This can be possibly explained in that the loaded platinum could stabilize the $SrTiO_3$ framework to a certain degree and increase the surface area due to its high dispersion on the $SrTiO_3$ surface. Even though the commercial $SrTiO_3$ and P-25 TiO_2 photocatalysts show no characteristic of the mesoporous structure, their surface areas are as high as 35.6 and 59.3 m^2/g, possibly due to their specific production processes. However, they exhibited comparatively lower photocatalytic hydrogen production activity, as described later.

Table 4.2 Summary of N_2 adsorption-desorption results of the synthesized mesoporous-assembled perovskite titanate photocatalysts and the commercial photocatalysts

Photocatalyst	Calcination temperature (°C)	Calcination time (h)	BET surface area ($m^2 \cdot g^{-1}$)	Mean mesopore diameter (nm)	Total pore volume ($cm^3 \cdot g^{-1}$)
$MgTiO_3$	450	4	134.8	4.65	0.280
	500		127.6	6.18	0.267
	550		71.6	8.87	0.257
	600		38.8	15.73	0.244
	650		31.5	15.84	0.254
$CaTiO_3$	500	4	35.8	6.12	0.136
	550		27.7	8.84	0.137
	600		21.3	8.83	0.120
	650		14.9	15.81	0.113
$SrTiO_3$	550	4	17.3	3.69	0.046
	600		14.4	3.63	0.038
	650		12.2	3.60	0.047
	700		10.9	3.62	0.041
0.5 wt.% Pt-loaded mesoporous-assembled $SrTiO_3$	650	4	18.8	8.80	0.057
Commercial $SrTiO_3$	-	-	35.6	-[a]	-[a]
Commercial P-25 TiO_2[b]	-	-	59.3	-[a]	-[a]

[a] N_2 adsorption-desorption isotherms correspond to IUPAC type II pattern.

[b] From Sreethawong *et al.* (2009)

4.1.3 XRD Results

XRD patterns of the mesoporous-assembled perovskite titanate photocatalysts ($MgTiO_3$ calcined at 450-650°C, $CaTiO_3$ calcined at 500-650°C, and $SrTiO_3$ calcined at 550-700°C) are shown in Figure 4.4. From the Figure 4.4(a), the dominant peaks of the rhombohedral $MgTiO_3$ at 2θ of about 32.9, 35.5, 40.6, 49.2, 53.6, 62.1, 63.7, and 71.1° represent the indices of (104), (110), (11$\bar{3}$), (024), (11$\bar{6}$), (12$\bar{4}$), (300) and (1010) planes (Smith, 1960), respectively. This crystalline phase was observed for the samples calcined between 550 and 650°C; however, at the calcination temperatures of 450 and 500°C, the amorphous phase was dominantly observed. The results suggested that the transition temperature of the $MgTiO_3$ for crystallizing to become the crystalline phase was around 500-550°C, which agrees well with the TG-DTA results (Figure 4.1(a)). Therefore, when the calcination temperature was increased from 500 to 550°C, the rhombohedral $MgTiO_3$ structure became the main crystalline phase. From Figure 4.4(b), the dominant peaks of the cubic $CaTiO_3$ at 2θ of about 33.2, 47.6, 59.2, 69.6, and 79.1° represent the indices of (110), (200), (211), (220), and (310) planes (Smith, 1960), respectively, and from Figure 4.4(c), the dominant peaks of the cubic $SrTiO_3$ at 2θ of about 32.4, 39.9, 46.4, 57.8, 67.8, and 77.2° represent the indices of (110), (111), (200), (211), (220), and (310) planes (Smith, 1960), respectively. As included in the Figure 4.4(c), the cubic $SrTiO_3$ structure was also observed for the commercial $SrTiO_3$ with slightly higher crystallinity than the synthesized $SrTiO_3$. The XRD pattern of the synthesized 0.5 wt.% Pt-loaded mesoporous-assembled $SrTiO_3$ photocatalyst calcined at 650°C is separately shown in Figure 4.5, for clarity. The dominant peak of Pt at 2θ of about 39.7° could not be clearly observed since its peak position is almost the same as a diffraction peak of the cubic $SrTiO_3$ phase. The existence of Pt will be confirmed by using TEM-EDX analyses, as explained later. In addition, the XRD pattern of the commercial P-25 TiO_2 photocatalyst is shown in Figure 4.6. The commercial P-25 TiO_2 shows the combined crystalline structure between the anatase and the rutile phases with approximately 26% rutile content (Sreethawong *et al.*, 2009). The phase identification and the crystallite size of all the investigated photocatalysts are summarized in Table 4.3.

(a)

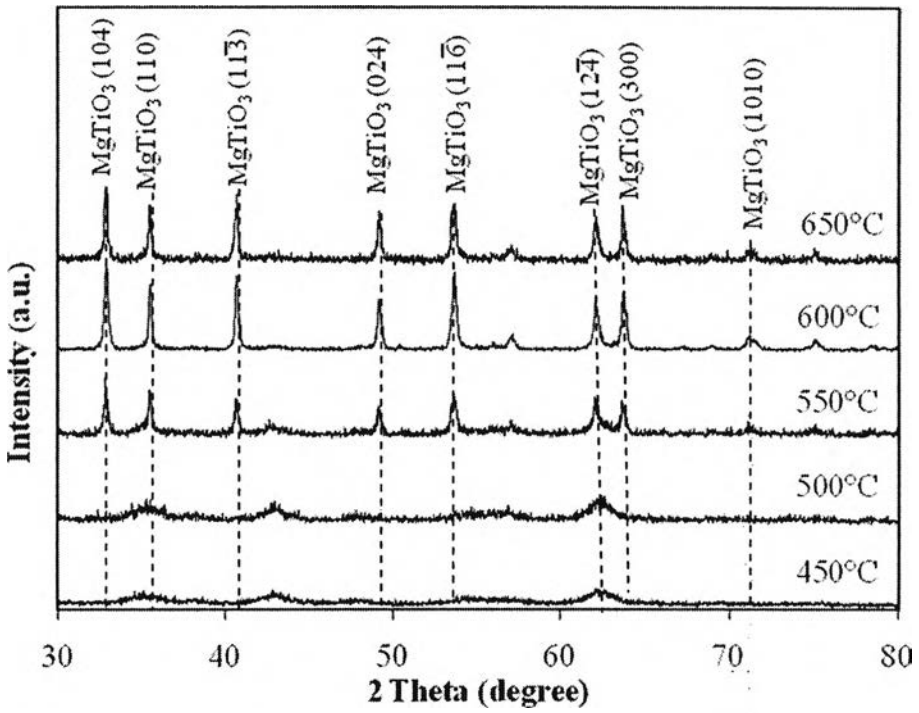

(b)

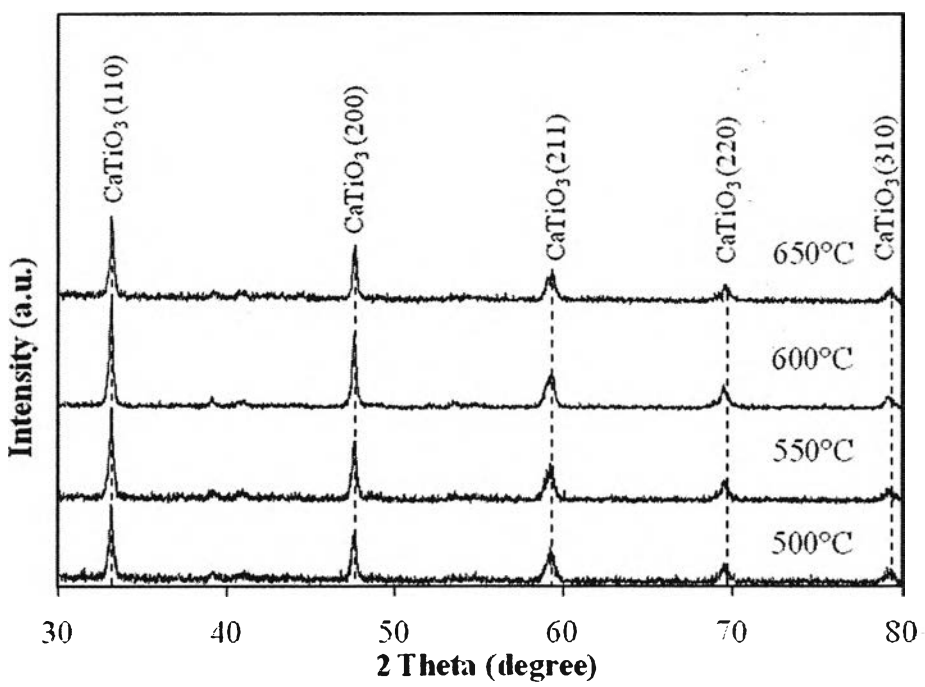

Figure 4.4 XRD patterns of the mesoporous-assembled (a) $MgTiO_3$ calcined at 450-650°C, (b) $CaTiO_3$ calcined at 500-650°C, and (c) $SrTiO_3$ calcined at 550-700°C and the commercial $SrTiO_3$.

(c)

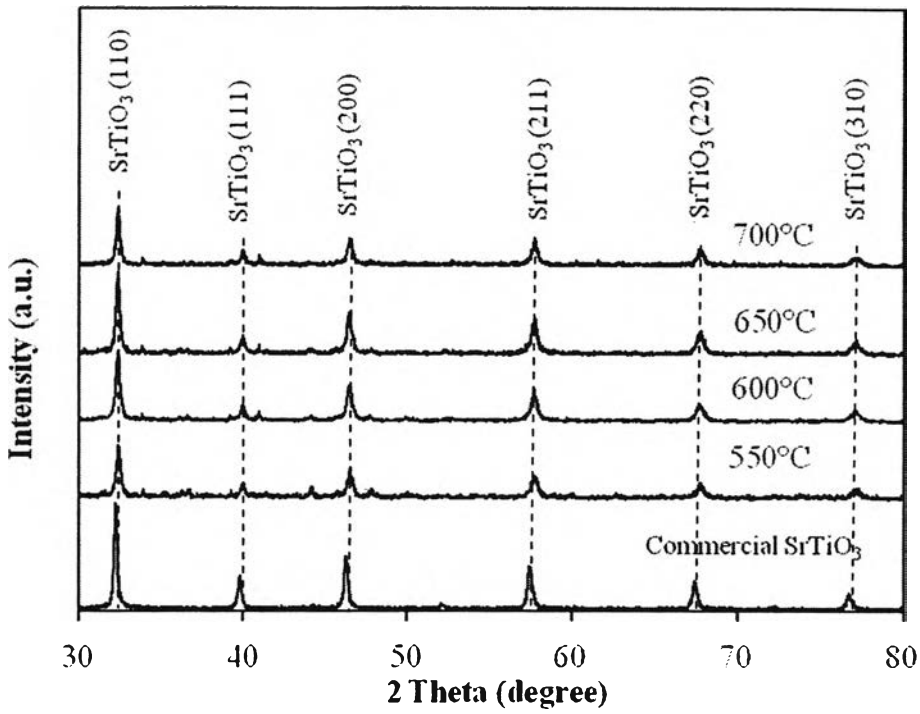

Figure 4.4 (Continued) XRD patterns of the mesoporous-assembled (a) $MgTiO_3$ calcined at 450-650°C, (b) $CaTiO_3$ calcined at 500-650°C, and (c) $SrTiO_3$ calcined at 550-700°C and the commercial $SrTiO_3$.

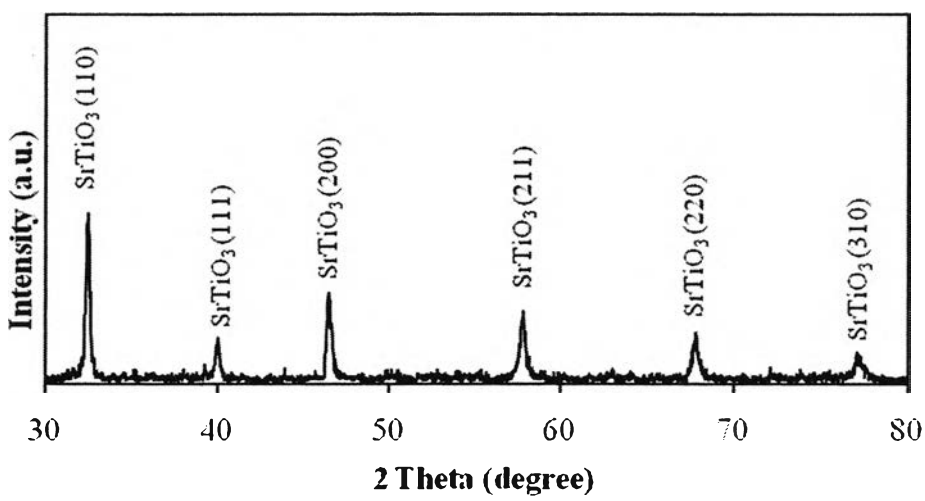

Figure 4.5 XRD pattern of the synthesized 0.5 wt.% Pt-loaded mesoporous-assembled $SrTiO_3$ calcined at 650°C.

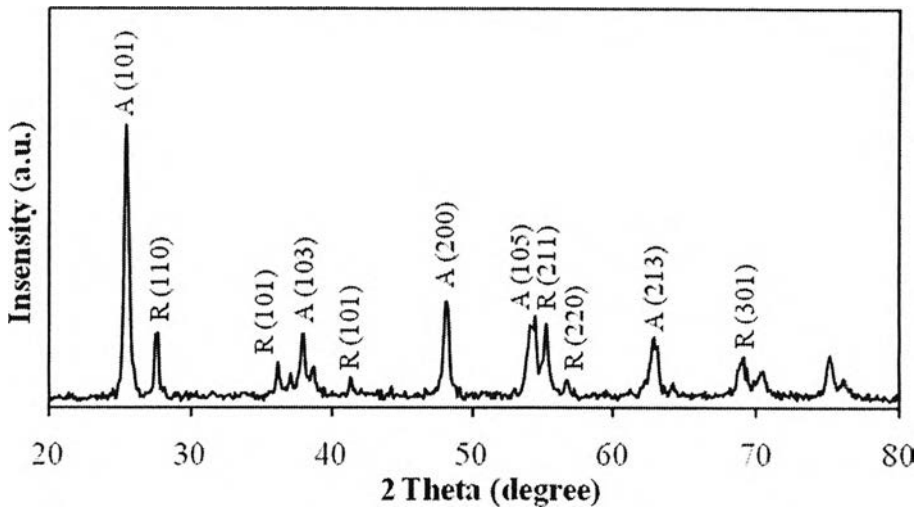

Figure 4.6 XRD pattern of the commercial P-25 TiO_2 photocatalyst (A: Anatase, R: Rutile).

Table 4.3 Summary of XRD analysis of the synthesized mesoporous-assembled perovskite titanate photocatalysts and the commercial photocatalysts

Photocatalyst	Calcination temperature (°C)	Calcination time (h)	Phase from XRD pattern	Crystallite size (nm)
$MgTiO_3$	450	4	Rhombohedral	-
	500			-
	550			29.38
	600			27.69
	650			30.59
$CaTiO_3$	500	4	Cubic	26.55
	550			28.88
	600			29.09
	650			29.09
$SrTiO_3$	550	4	Cubic	27.39
	600			27.57
	650			30.44
	700			31.61

Photocatalyst	Calcination Temperature (°C)	Calcination time (h)	Phase from XRD pattern	Crystallite size (nm)
0.5 wt.% Pt-loaded mesoporous-assembled $SrTiO_3$	650	4	Cubic	28.33
Commercial $SrTiO_3$	-	-	Cubic	30.54
Commercial P-25 TiO_2[(a)]	-	-	Anatase + Rutile	22.00 (Anatase) 28.90 (Rutile)

[(a)] From Sreethawong *et al.* (2009)

The crystallite size of the photocatalysts was calculated from the line broadening of the most preferentially formed X-ray diffraction peak of each crystalline phase according to the Sherrer equation (Cullity, 1978) (Eq. 4.1):

$$L = \frac{k\lambda}{\beta \cos(\theta)} \tag{4.1}$$

where L is the crystallite size, k is the Sherrer constant usually taken as 0.89, λ is the wavelength of the X-ray radiation (0.15418 nm for Cu Kα), β is the full width at half maximum (FWHM) of the diffraction peak measured at 2θ, and θ is the diffraction angle. From Table 4.3, the crystallite sizes of all the perovskite titanate photocatalysts are about 27-31 nm. The results clearly reveal that with increasing calcination temperature, the larger crystallite size of the photocatalysts was obtained. It is interestingly observed that the crystallite size of the Pt-loaded $SrTiO_3$ is lower than that of the unloaded $SrTiO_3$. This implies the role of Pt in stabilizing the $SrTiO_3$ framework from coalescence upon the calcination, as aforementioned, leading to the obtained higher surface area (Table 4.2).

4.1.4 UV-visible Spectroscopy Results

UV-visible spectroscopy was used to examine the light absorption ability of the synthesized mesoporous-assembled perovskite titanate photocatalysts,

as well as Eosin Y (E.Y.) solution used as a sensitizer for the photocatalytic H_2 production. Figure 4.7 shows the UV-visible spectra of the mesoporous-assembled $MgTiO_3$ calcined at 450-650°C, $CaTiO_3$ calcined at 500-650°C, and $SrTiO_3$ calcined at 550-700°C. The results of onset absorption wavelength and corresponding band gap energy of all the photocatalysts obtained from the UV-visible spectra are summarized in Table 4.4. It is clearly seen that the absorption band of the mesoporous-assembled perovskite titanate photocatalysts are in the UV light range of 200-400 nm. The band gap energy (E_g, eV) is determined by extrapolating the onset of the rising part to x-axis (λ_g, nm) of the plots, as shown by dotted lines in Figure 4.7, and calculated by Eq. (4.2).

$$E_g = \frac{1240}{\lambda_g} \tag{4.2}$$

where λ_g is the wavelength (nm) of the exciting light. The band gap energies of the mesoporous-assembled $MgTiO_3$ calcined at 450-650°C, $CaTiO_3$ calcined at 500-650°C, and $SrTiO_3$ calcined at 550-700°C are approximately 3.35 eV ($\lambda_g \sim 370$ nm), 3.55 eV ($\lambda_g \sim 349$ nm), and 3.22 eV ($\lambda_g \sim 385$ nm), respectively. From the results, it is clearly observed that $SrTiO_3$ has comparatively the narrowest band gap energy, implying that $SrTiO_3$ can be excited by the lowest energy level. However, it can be noticed from the light absorption ability of all the investigated perovskite titanate photocatalysts that they could absorb only UV light with wavelength shorter than 400 nm. The comparative results from UV-visible spectra of the mesoporous-assembled $SrTiO_3$ calcined at 650°C, the synthesized 0.5 wt.% Pt-loaded mesoporous-assembled $SrTiO_3$ calcined at 650°C, and the commercial $SrTiO_3$ are shown in Figure 4.8. The band gap energy of the synthesized 0.5 wt.% Pt-loaded mesoporous-assembled $SrTiO_3$ is approximately 3.12 eV ($\lambda_g \sim 398$ nm), which becomes closer to the energy of visible light. Moreover, it has more visible light absorption ability than the mesoporous-assembled $SrTiO_3$ and the commercial $SrTiO_3$.

(a)

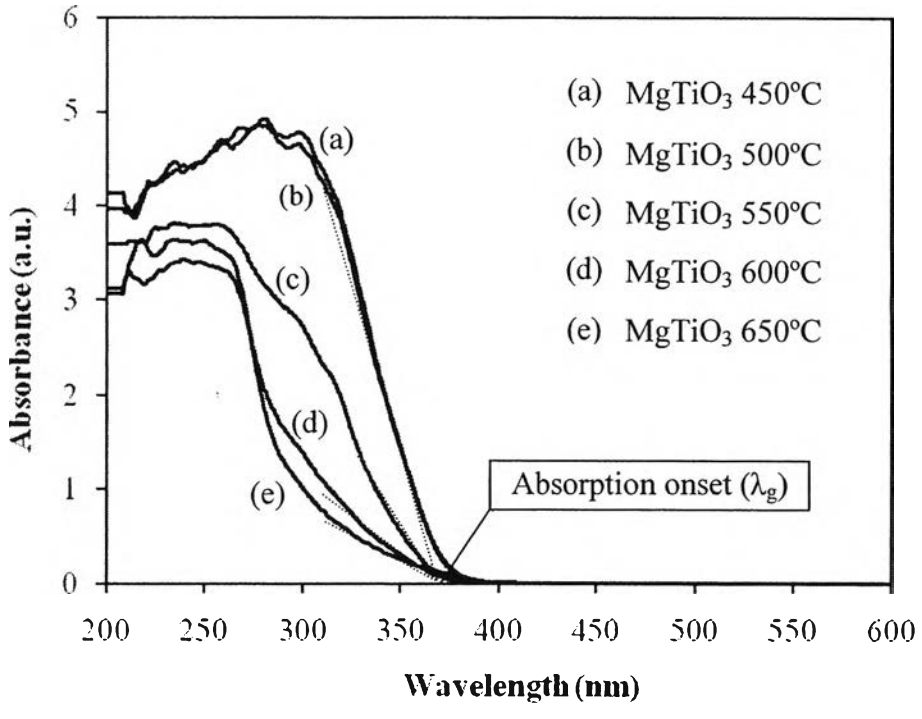

(b)

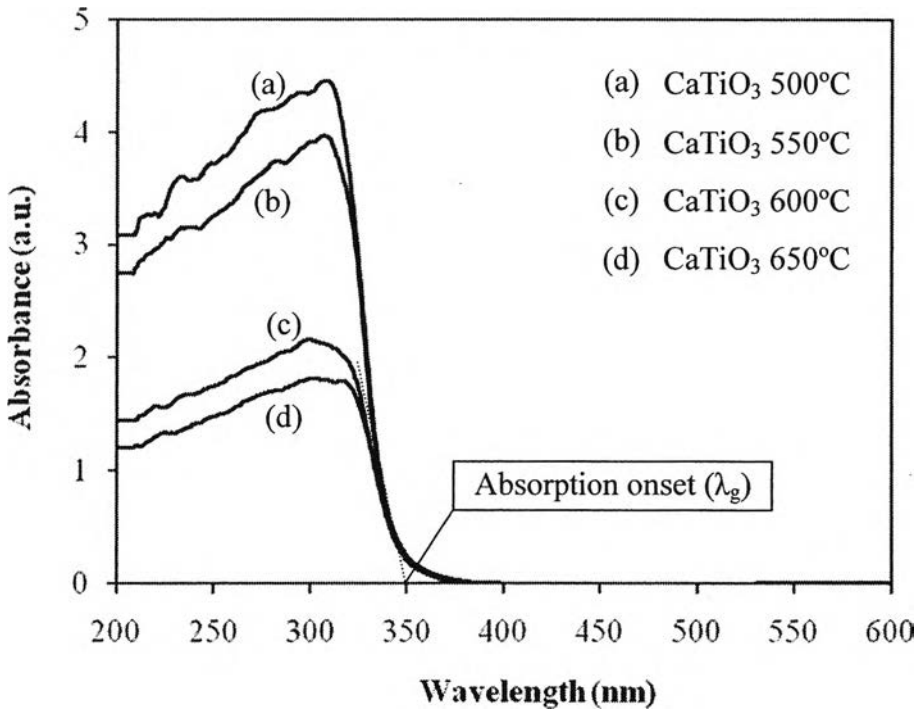

Figure 4.7 UV-visible spectra of the mesoporous-assembled (a) $MgTiO_3$ calcined at 450-650°C, (b) $CaTiO_3$ calcined at 500-650°C, and (c) $SrTiO_3$ calcined at 550-700°C.

(c)

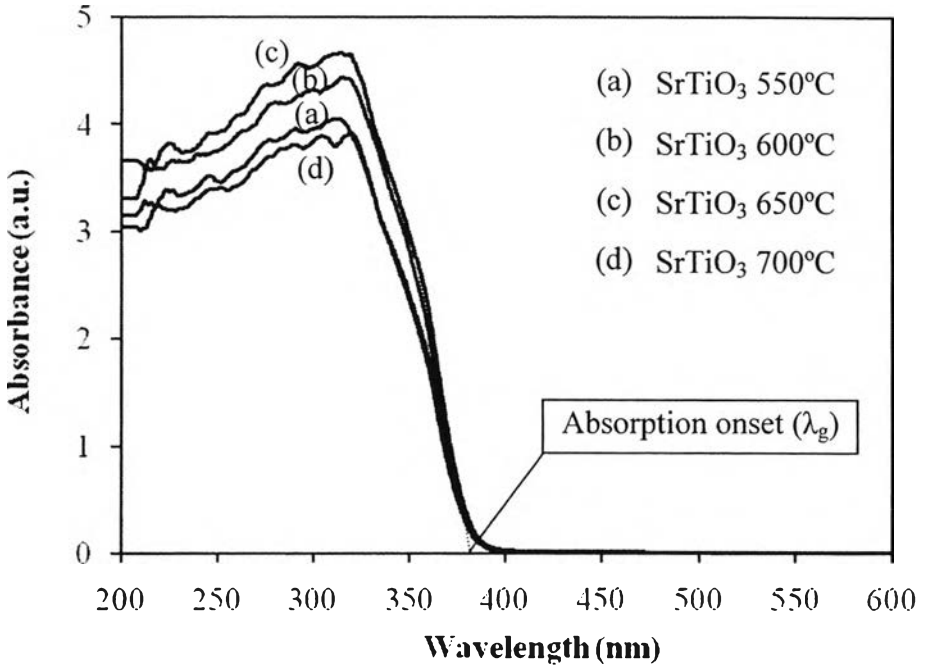

Figure 4.7 (Continued) UV-visible spectra of the mesoporous-assembled (a) $MgTiO_3$ calcined at 450-650°C, (b) $CaTiO_3$ calcined at 500-650°C, and (c) $SrTiO_3$ calcined at 550-700°C.

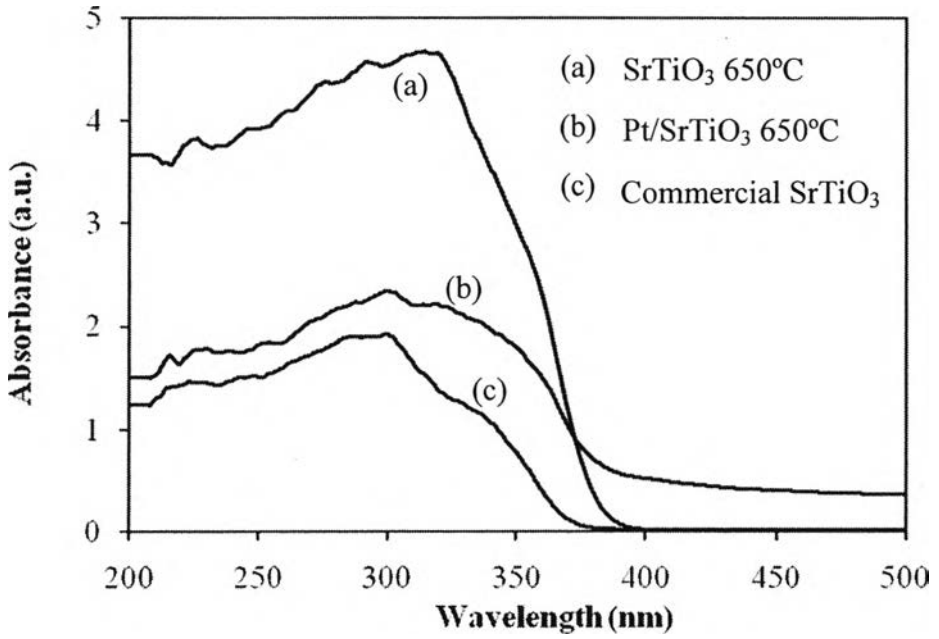

Figure 4.8 UV-visible spectra of (a) the mesoporous-assembled $SrTiO_3$ calcined at 650°C, (b) the 0.5 wt.% Pt-loaded mesoporous-assembled $SrTiO_3$ calcined at 650°C, and (c) the commercial $SrTiO_3$.

Table 4.4 Summary of onset absorption wavelength and band gap energy of the synthesized mesoporous-assembled perovskite titanate photocatalysts and the commercial photocatalysts

Photocatalyst	Calcination temperature (°C)	Calcination time (h)	Onset absorption wavelength, λ_g (nm)	Band gap energy (eV)
$MgTiO_3$	450	4	370	3.35
	500		370	3.35
	550		368	3.37
	600		370	3.35
	650		370	3.35
$CaTiO_3$	500	4	349	3.55
	550		349	3.55
	600		345	3.59
	650		345	3.59
$SrTiO_3$	550	4	385	3.22
	600			
	650			
	700			
0.5 wt.% Pt-loaded mesoporous-assembled $SrTiO_3$	650	4	398	3.12
Commercial $SrTiO_3$	-	-	360	3.44
Commercial P-25 TiO_2[(a)]	-	-	390	3.18

[(a)] From Sreethawong *et al.* (2009)

In order to confirm that Eosin Y (E.Y.) is the visible light-responding sensitizer, its UV-visible spectrum was also measured, as shown in Figure 4.9. It is clear that E.Y. could mainly absorb the visible light with the maximum absorption centered at 516 nm. This absorption feature strongly suggests that the sensitizer can be activated by the visible light for the sensitized photocatalytic hydrogen production system in this study.

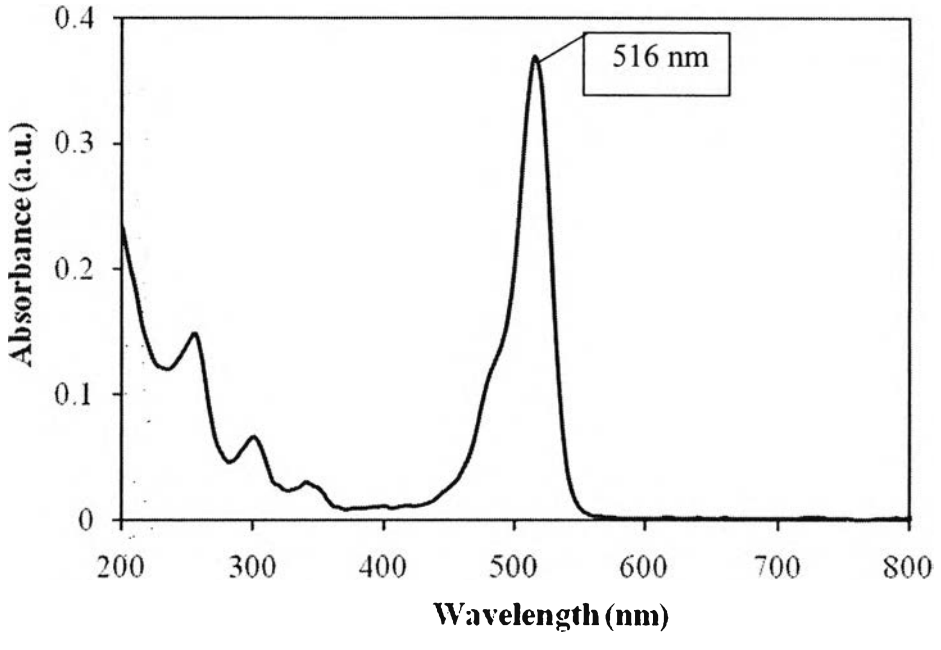

Figure 4.9 UV-visible spectrum of Eosin Y solution.

4.1.5 TEM Results

The morphologies of all the synthesized mesoporous-assembled perovskite titanate photocatalysts were investigated by TEM. Figure 4.10 shows the exemplified TEM images of the synthesized $MgTiO_3$ calcined at 500°C, the $CaTiO_3$ calcined at 550°C, and the $SrTiO_3$ calcined at 650°C, which exhibited the highest photocatalytic activity for each perovskite series. The average particle sizes of $MgTiO_3$, $CaTiO_3$, and $SrTiO_3$ are approximately in the range of 5-15, 20-35, and 20-35 nm, respectively. It can be observed that the particle sizes of the crystalline photocatalysts agree well with the crystallite sizes calculated from XRD patterns by the Scherrer equation. The similar results for the other samples prepared at different conditions can be reasonably analogous as well. In order to obtain the particle size of Pt, the high resolution TEM (HRTEM) and the EDX mapping of the synthesized 0.5

wt.% Pt-loaded mesoporous-assembled $SrTiO_3$ calcined at 650°C were performed, and the results are shown in Figure 4.11. The Pt nanoparticle is clearly seen as dark patches, indicating high electron density, as confirmed by the EDX mapping. The average particle size of Pt is in the range of 5-15 nm.

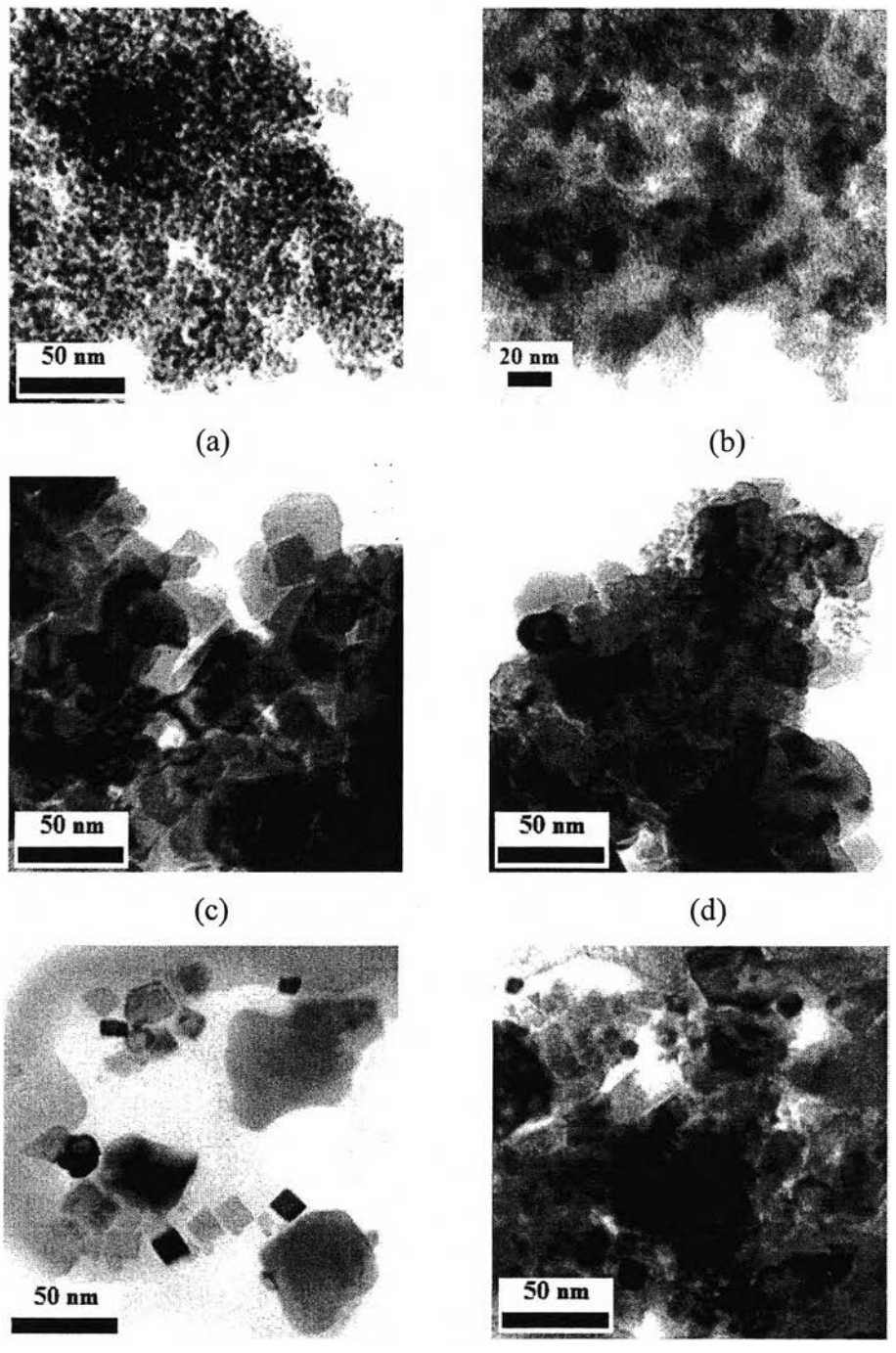

Figure 4.10 TEM images of the synthesized (a,b) $MgTiO_3$ calcined at 500°C, (c,d) $CaTiO_3$ calcined at 550°C, and (e,f) $SrTiO_3$ calcined at 650°C.

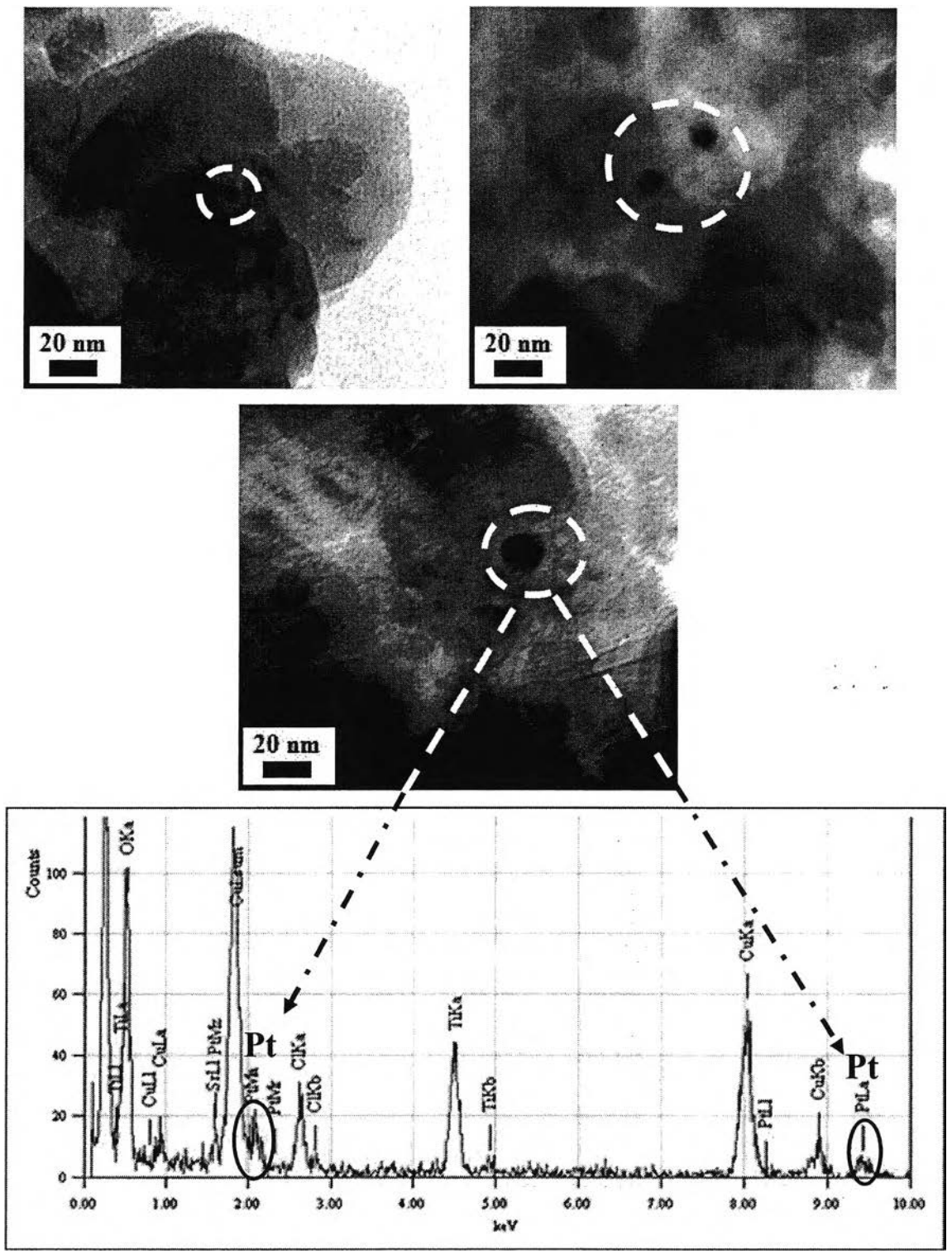

Figure 4.11 H igh resolution TEM (HRTEM) image and EDX elemental point mapping of the 0.5 wt.% Pt-loaded mesoporous-assembled $SrTiO_3$ calcined at 650°C.

4.2 Sensitized Photocatalytic Hydrogen Production Activity

In this study, the photocatalytic activity of the synthesized mesoporous-assembled perovskite titanate photocatalysts calcined at various calcination temperatures was first investigated for the sensitized hydrogen production from aqueous DEA solution containing E.Y. sensitizer under visible light irradiation. The photocatalytic activity in the absence of either light irradiation, photocatalyst, E.Y., or DEA was also comparatively studied. It was experimentally found that there was no appreciable H_2 production in the absence of either of them. Besides, it was observed that the photolysis process (the light-irradiated system without a photocatalyst) could generate only negligibly small amount of hydrogen. The effective way to improve the amount of produced hydrogen was to add a photocatalyst to the aqueous solution of E.Y. and DEA. Briefly about the mechanism of the sensitized photocatalytic hydrogen production, under irradiation by visible light, the sensitizer is excited into its excited state. Then, the excited sensitizer can inject electrons to the conduction band of perovskite titanate photocatalysts to initiate the catalytic reaction. Finally, the excited electrons in the perovskite titanate conduction band can rapidly transport to the loaded Pt cocatalyst active sites, which are deposited on the surface of perovskite titanate photocatalysts, and reduce protons in the solution to generate the hydrogen. In order to regenerate the sensitizer, the oxidized-state sensitizer can be reduced by the electron donor (DEA), and return into the ground-state sensitizer.

4.2.1 Effect of Photocatalyst Type

In this photocatalytic reaction, 0.2 g of different types of the mesoporous-assembled perovskite titanate photocatalysts were suspended in 150 ml of 15 vol.% DEA aqueous solution (22.5 ml DEA and 127.5 ml distilled water) containing dissolved 0.1 mM E.Y. at room temperature, and the mixture was used for the photocatalytic reaction. The results of hydrogen production rate of the mesoporous-assembled $MgTiO_3$ (calcined at 450, 500, 550, 600, and 650°C), $CaTiO_3$ (calcined at 500, 550, 600, and 650°C), and $SrTiO_3$ (calcined at 550, 600, 650 and 700°C) photocatalysts are shown in Figure 4.12

(a)

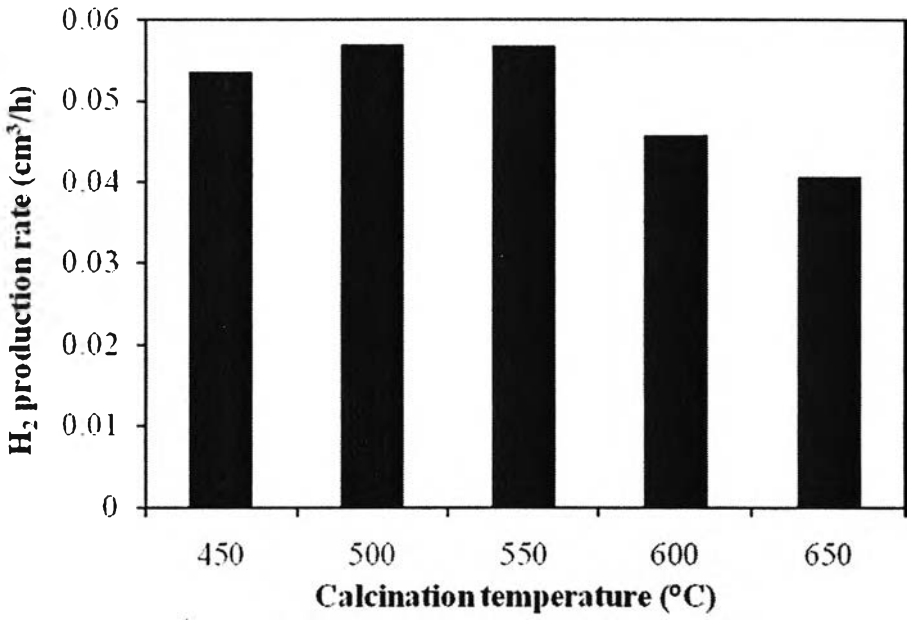

(b)

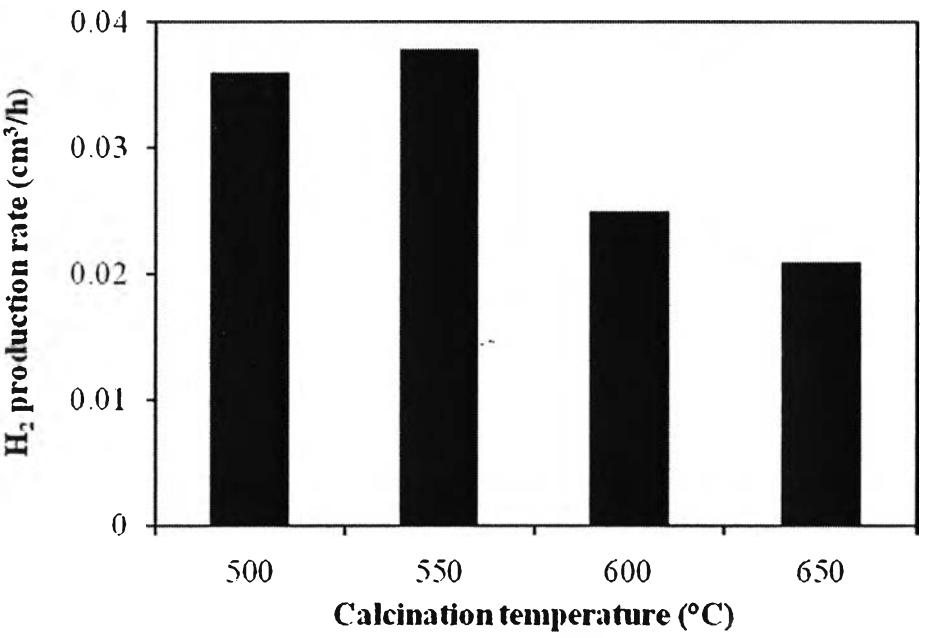

Figure 4.12 Effect of calcination temperature of the mesoporous-assembled (a) $MgTiO_3$, (b) $CaTiO_3$, and (c) $SrTiO_3$ photocatalysts on hydrogen production activity (Photocatalyst, 0.2 g; total volume, 150 ml; DEA concentration, 15 vol.%; E.Y. concentration, 0.1 mM; initial solution pH, 11.6; irradiation time, 5 h).

(c)

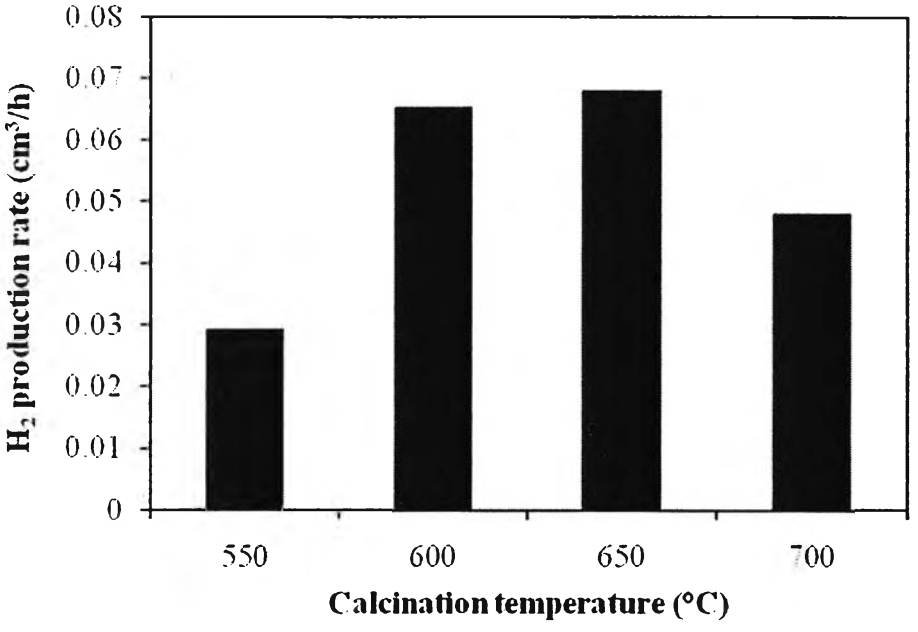

Figure 4.12 (Continued) Effect of calcination temperature of the mesoporous-assembled (a) $MgTiO_3$, (b) $CaTiO_3$, and (c) $SrTiO_3$ photocatalysts on hydrogen production activity (Photocatalyst, 0.2 g; total volume, 150 ml; DEA concentration 15 vol.%; E.Y. concentration, 0.1 mM; initial solution pH, 11.6; irradiation time, 5 h).

From Figure 4.12, it can be seen that the hydrogen production rate of the mesoporous-assembled $MgTiO_3$, $CaTiO_3$, and $SrTiO_3$ photocatalysts calcined at 500, 550, and 650°C, respectively, were much higher than those in each perovskite series calcined at other temperatures. Among the investigated photocatalysts calcined at their optimum temperatures, the mesoporous-assembled $SrTiO_3$ photocatalyst provided the highest photocatalytic activity (0.068 cm^3/h) because it possesses the narrowest band gap energy (Table 4.4). Therefore, it has the highest driving force for the electron transfer from the excited E.Y. to its conduction band. The photocatalytic activity of the $MgTiO_3$ photocatalyst was lower than that of the $SrTiO_3$ photocatalyst possibly because the easily formed defect titanate center within the $MgTiO_3$ sublattice acts as a recombination center (De Haart *et al.*, 1984). Even though the $CaTiO_3$ photocatalyst could produce hydrogen from the sensitized photocatalytic water splitting, its photocatalytic activity was lower than that of the

$SrTiO_3$ photocatalyst, as also observed by Zielińska *et al.* (2008). Figure 4.13 shows the comparison of the hydrogen production rates of the mesoporous-assembled $MgTiO_3$, $CaTiO_3$, and $SrTiO_3$ photocatalysts calcined at their optimum temperatures, as compared to the 0.5 wt.% Pt-loaded mesoporous-assembled $SrTiO_3$ photocatalyst calcined at 650°C and the commercial $SrTiO_3$ and P-25 TiO_2 photocatalysts. It was found that when Pt nanoparticles of 0.5 wt.% loading content acting as the active sites were deposited on the mesoporous-assembled $SrTiO_3$ photocatalyst surface, the rate of sensitized photocatalytic hydrogen production was enhanced remarkably from 0.068 to 0.33 cm^3/h, being the highest photocatalytic activity among all the photocatalysts investigated. This confirms that the Pt loading can be employed to greatly improve the hydrogen production rate. In addition, the mesoporous-assembled $SrTiO_3$ photocatalyst calcined at 650°C experimentally provided higher hydrogen production rate than both the commercial $SrTiO_3$ and the P-25 TiO_2 photocatalysts possibly because it predominantly possesses the mesoporous characteristic with narrow pore size distribution in the mesoporous range between 2 and 50 nm (Figure 4.2), whereas both the commercial photocatalysts posseses mostly the macropore characteristic with broad pore size distributions extended into the macroporous range larger than 50 nm (Figure 4.3). This implies the significance of the mesoporous structure of the photocatalyst for the photocatalytic hydrogen production activity.

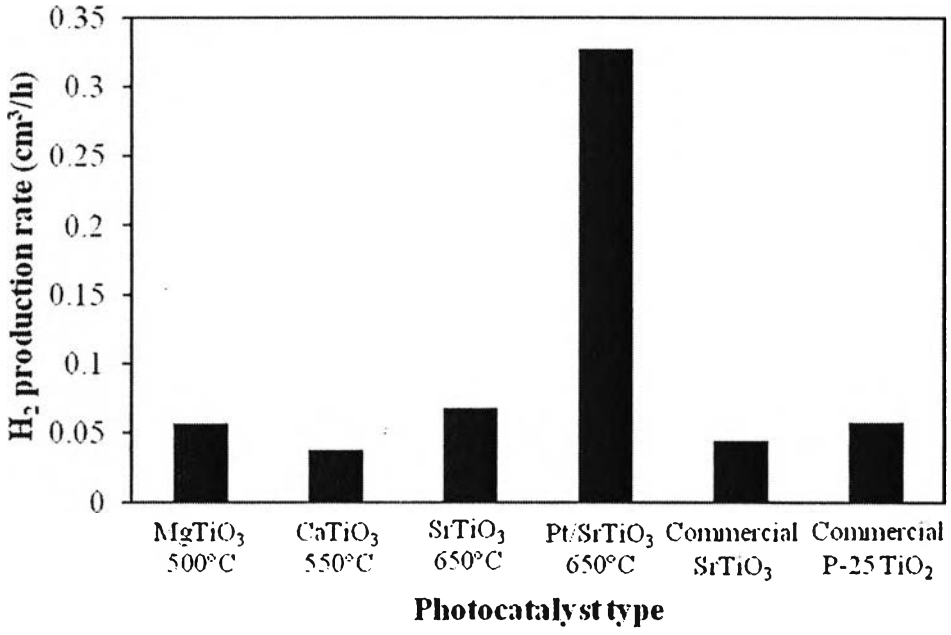

Figure 4.13 Effect of photocatalyst type on hydrogen production activity (Photocatalyst, 0.2 g; total volume, 150 ml; DEA concentration, 15 vol.%; E.Y. concentration, 0.1 mM; initial solution pH, 11.6; irradiation time, 5 h).

4.2.2 Effect of Electron Donor Type and Concentration

In the photosensitized hydrogen production system, the electron donors or sacrificial reagents, which were DEA and TEA in this study, could play an important role in regenerating the electron-deficient sensitizer (oxidized sensitizer). In order to obtain higher photosensitized efficiency in converting absorbed light into hydrogen energy, fast electron injection and slow backward reaction are required. Thus, the effect of type and concentration of electron donor working as the sensitizer regenerator needs to be studied. As clearly seen from the previous that the 0.5 wt.% Pt-loaded mesoporous-assembled $SrTiO_3$ calcined at 650°C showed the highest performance for the photocatalytic hydrogen production, it was used as the photocatalyst to investigate the effect of electron donor type and concentration on the sensitized photocatalyst activity in this part. Figure 4.14 shows the photocatalytic hydrogen production activity of the synthesized 0.5 wt.% Pt-loaded mesoporous-assembled $SrTiO_3$ photocatalyst using either DEA or TEA at various concentrations.

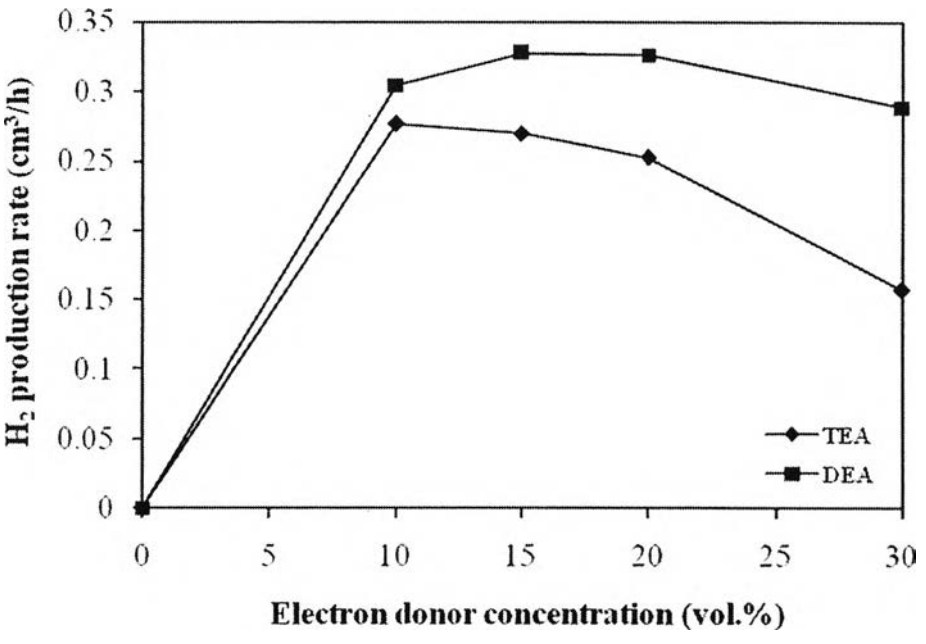

Figure 4.14 Effect of electron donor type and concentration on hydrogen production activity over the 0.5 wt.% Pt-loaded mesoporous-assembled $SrTiO_3$ calcined at 650°C (Photocatalyst, 0.2 g; total volume, 150 ml; E.Y. concentration, 0.1 mM; initial solution pH, 11.0-11.6; irradiation time, 5 h).

The results show that no hydrogen production was observed under visible light irradiation from the E.Y.-containing system without dissolved DEA or TEA. Moreover, when the DEA or TEA concentration increased, the photocatalytic hydrogen production increased until reaching the maximum at 15 and 10 vol.%, respectively, exhibiting the hydrogen production rate about 0.33 and 0.28 cm^3/h, respectively. The further increase in their concentrations negatively affected the hydrogen production rate. It was found that at any given concentration, the DEA more positively affected the hydrogen production rate than the TEA, as also observed by Jin *et al.*, 2006. This might be attributable to a higher electron-donating ability of N atom in the DEA molecule than that in the TEA molecule because of less bulky molecular structure of the DEA due to shorter chain length of the hydrocarbon part. When using methanol instead of DEA or TEA no hydrogen production was observed under visible light irradiation. Normally, methanol is an effective electron donor for the photocatalytic water splitting under UV light

irradiation, where it scavenges the directly photogenerated holes at the photocatalyst valence band. However, in this system, methanol did not work as the electron donor at all, supporting that the hydrogen production originates from the water reduction by the electrons from the excited sensitizer, not from the electrons generated in the photocatalyst by direct light absorption, resulting in no holes produced in the photocatalyst (Hirano *et al.*, 2000). By focusing on the DEA, 15 vol.% DEA was found to be the optimum concentration for efficient hydrogen production. When further increasing DEA concentration beyond the optimum level, the hydrogen production rate did not increase. This is probably because the DEA concentration of 15 vol.% was effectively sufficient for regenerating or quenching excited sensitizer and also preventing the electron-excited sensitizer recombination. Therefore, excess DEA in the system was not required. Since 15 vol.% DEA was experimentally verified to be the most suitable electron donor concentration for the investigated system, it was used as the main studied electron donor concentration in further experiments.

4.2.3 Effect of Sensitizer Concentration

The concentration of E.Y. plays a significant role in the number of electrons transferring from the excited E.Y. to the conduction band of the perovskite titanates to enhance the photocatalytic hydrogen production. In this part, the 0.5 wt.% Pt-loaded mesoporous-assembled $SrTiO_3$ suspended in 150 ml of 15 vol.% DEA aqueous solution containing dissolved E.Y was used to investigate the effect of E.Y. concentration on the sensitized photocatalytic activity. Figure 4.15 shows the effect of dissolved E.Y. concentration (varied from 0 to 1 mM) on the photocatalytic production of hydrogen. The results show that the rate of photocatalytic hydrogen production significantly increased with increasing E.Y. concentration and reached a maximum at 0.5 mM (hydrogen production rate of about 1.01 cm^3/h). However, with further increasing E.Y. concentration beyond 0.5 mM, the hydrogen production rate decreased. To explain this behavior, only the fraction of the sensitizer adsorbed on the $SrTiO_3$ surface must be first considered to be photocatalytically active with respect to the electron injection into the conduction band of the $SrTiO_3$ photocatalyst (Dhanalakshmi *et al.*, 2000). Initially, with the increase in the sensitizer

concentration, such the fraction increased, hence the hydrogen production rate was significantly increased. If all the photocatalytically active sites are adsorbed by the sensitizer, there is no further increase in the hydrogen production rate with further increasing sensitizer concentration due to a saturation limit of the sensitizer adsorption sites. Thus, with the further increase in the E.Y. concentration beyond the optimum value of 0.5 mM, the number of adsorbed E.Y. hardly increases. In addition, the excess E.Y. in the solution can be excited, but cannot inject electrons to the photocatalyst conduction band for participating in the photocatalytic reaction. This also leads to less light absorption of the E.Y. adsorbed at the photocatalyst surface, resulting in lowering the photocatalytic activity at too high E.Y. concentration.

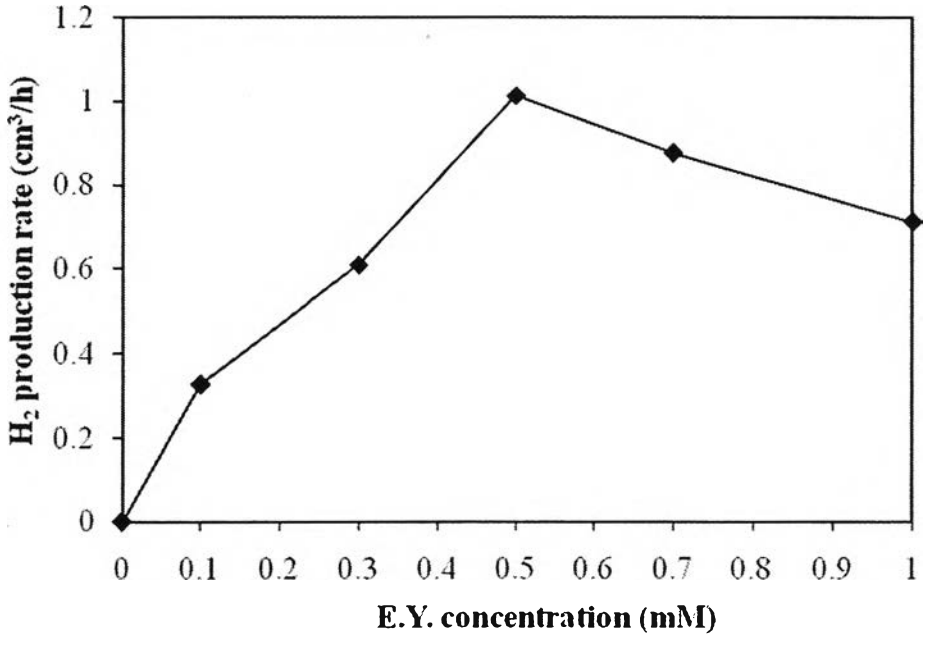

Figure 4.15 Effect of E.Y. concentration on hydrogen production activity over the 0.5 wt.% Pt-loaded mesoporous-assembled $SrTiO_3$ calcined at 650°C (Photocatalyst, 0.2 g; total volume, 150 ml; DEA concentration, 15 vol.%; initial solution pH, 11.6; irradiation time, 5 h).

4.2.4 Effect of Photocatalyst Dosage

The effect of the dosage of the synthesized 0.5 wt.% Pt-loaded mesoporous-assembled $SrTiO_3$ photocatalyst suspended in the 15 vol.% DEA

aqueous solution containing dissolved 0.5 mM E.Y. on the photocatalytic hydrogen production was next investigated. In this study, the photocatalyst dosage was varied in the range of 0 to 10 g/l by adjusting amount of the photocatalyst added to the photocatalytic reactor under the identical solution conditions. Figure 4.16 shows the effect of the photocatalyst dosage on the rate of hydrogen production. The results show that the photocatalyst dosage of 6 g/l provided the maximum hydrogen production rate of about 1.35 cm^3/h. Below or above this dosage, a decrease in the rate of hydrogen production was observed.

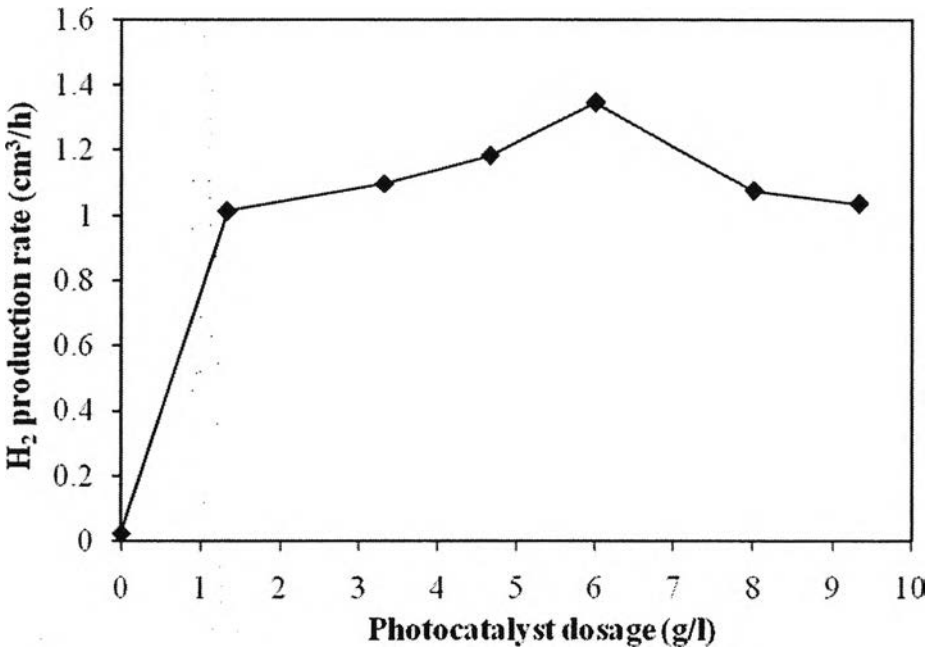

Figure 4.16 Effect of photocatalyst dosage on hydrogen production activity over the 0.5 wt.% Pt-loaded mesoporous-assembled $SrTiO_3$ calcined at 650°C (Total volume, 150 ml; DEA concentration, 15 vol.%; E.Y. concentration, 0.5 mM; initial solution pH, 11.6; irradiation time, 5 h).

A higher dosage of the photocatalyst is expected to correspond to a greater absorption of visible light energy, leading to a higher photocatalytic hydrogen production activity. However, the photocatalytic activity started to decline when the dosage of the photocatalyst exceeded the optimum value, indicating that the added amount of the photocatalyst has to be optimized. The results can be

explained in the terms of the availability of the active sites on the photocatalyst surface and the penetration of photoactivating light into the suspension (Konstantinou and Albanis, 2004). As the photocatalyst concentration increases, the availability of active sites also increases, but the light penetration and the subsequent photoactivated volume of the suspension decrease. The irradiating light could not penetrate throughout the reactor because of the covering by large quantity of the photocatalyst in the aqueous solution. The large crowd of the photocatalyst shielded the further penetration of light into the center the reactor, resulting in blocking the irradiating light. Although the light absorption of the outer photocatalyst increased, the capability of hydrogen production from the inner photocatalyst decreased due to the lack of photoexcitation. Moreover, deactivation of the active photocatalyst molecules due to the agglomeration and sedimentation of the photocatalyst particles and the consequent decrease in photocatalytic activity have also been reported (Konstantinou and Albanis, 2004). The optimum amount of the photocatalyst was required for the system in order to avoid unnecessary excess photocatalyst and also to assure total absorption of light photons for the efficient photocatalytic hydrogen production reaction.

4.2.5 Effect of Initial Solution pH

One of the important parameters affecting on the photosensitized hydrogen production is the solution pH. The role of initial solution pH on the photocatalytic hydrogen production was studied in the pH range of 8.4 -12.6 using DEA as an electron donor, noting that the initial pH of the original 15 vol.% DEA aqueous solution was approximately 11.6, and insignificant changes of solution pH were observed after the courses of the photocatalytic reaction. Figure 4.17 shows the effect of the initial solution pH on the rate of hydrogen production. The experimental results indicate that the hydrogen production activity increased with increasing initial solution pH from 8.4 to 11.6, and a further increase in the initial solution pH greater than 11.6 led to a decrease in the hydrogen production activity. The results imply that the hydrogen production activity of the photosensitized system was favorable at nearly strong basic solution, and the optimum initial solution pH was around 11.6. A possible explanation is that the pH value of the solution could affect

the DEA oxidation reaction. It has been reported that hydrogen production increased as the solution pH increased, especially sharply at pH > 6 (Malinka and Kamalov, 1994). This is because amine is more rapidly oxidized in alkaline solution since the oxidation constant of the amine is lower in an acidic solution owing to the fact that the amine is protonated. Consequently, the rate of regeneration of the sensitizer could be enhanced in an alkaline solution. Therefore, the unfavorable back reaction of excited sensitizer would be retarded, and the efficiency of the utilization of excited sensitizer would be improved. Finally, the rate of hydrogen production was remarkably enhanced. However, when the initial solution pH was beyond the optimum value (too alkaline), the complexity of coulombic repulsion/interaction among OH^-, DEA, sensitizer, and photocatalyst surface might play a negative role in reducing the overall photocatalytic activity.

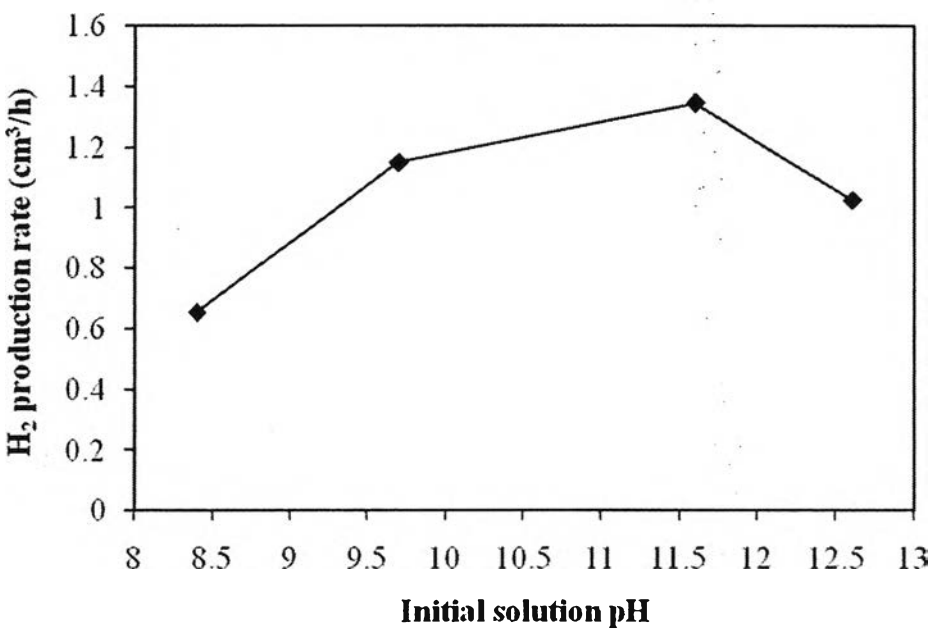

Figure 4.17 Effect of initial solution pH on hydrogen production activity over the 0.5 wt.% Pt-loaded mesoporous-assembled $SrTiO_3$ calcined at 650°C (Photocatalyst, 0.9 g; total volume, 150 ml; DEA concentration, 15 vol.%; E.Y. concentration, 0.5 mM; initial solution pH, 11.6; irradiation time, 5 h).

4.2.6 Photocatalyst Durability

The photocatalyst durability in the sensitized hydrogen production system was investigated. The obtained optimum conditions were employed for the

photocatalyst durability test. At the end of 5 h irradiation of the first run, the photocatalytic system was evacuated by Ar bubbling and again immediately used for the second run. This procedure was repeated to study the photocatalytic activity of the sensitized 0.5 wt.% Pt-loaded mesoporous-assembled $SrTiO_3$ photocatalyst for 3 consecutive runs. The E.Y. concentration was not significantly changed during the photocatalyst durability test. The results in Figure 4.18 show that the photocatalytic hydrogen production rates for the 3 consecutive runs are 1.38, 1.24, and 0.71 cm^3/h, respectively. It can be seen that the hydrogen production rate for the second run was slightly lower than that of the first run, but that of the third run decreased significantly as almost a half as that of the first and second runs. A large decrease in the photocatalytic hydrogen production rate for the third run might possibly originate from strong adsorption of many species, such as inactive E.Y. and DEA, on the photocatalyst surface, especially on the Pt active sites. An effective way to maintain the photocatalytic activity for several consecutive runs or long-period irradiation needs to be further investigated; otherwise, the photocatalyst replacement is required.

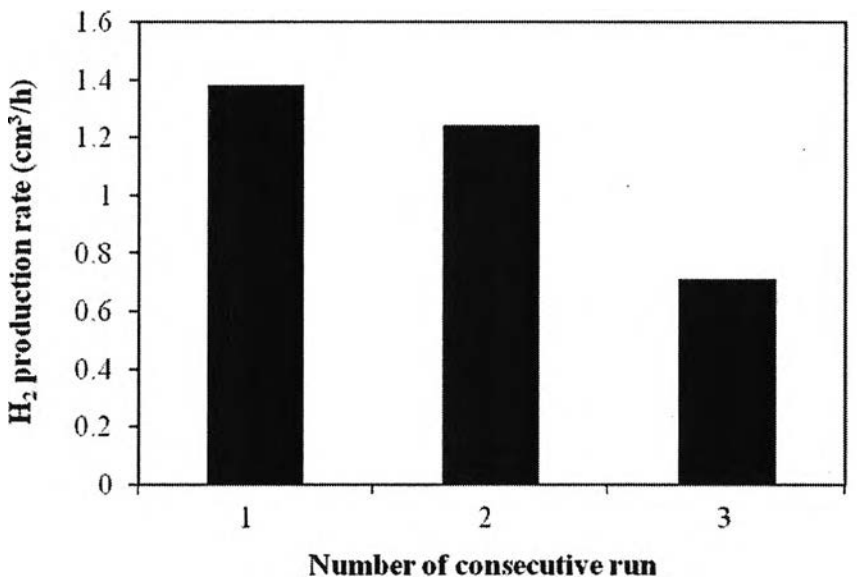

Figure 4.18 Durability of the 0.5 wt.% Pt-loaded mesoporous-assembled $SrTiO_3$ calcined at 650°C in the sensitized hydrogen production system for 3 consecutive runs (Photocatalyst, 0.9 g; total volume 150 ml; DEA concentration, 15 vol.%; E.Y. concentration, 0.5 mM; initial solution pH, 11.6; irradiation time for each run, 5 h).